Available online at www.sciencedirect.com
ScienceDirect
International Journal of Thermal Sciences 46 (2007) 1163–1171
International Journal of Thermal Sciences
www.elsevier.com/locate/ijts

Experimental investigation on flow and thermal characteristics of a micro phase-change cooling system with a microgroove evaporator

Xuegong Hu *, Dawei Tang

Institute of Engineering Thermophysics, Chinese Academy of Sciences, P.O. Box 2706, Beijing 100080, PR China

Received 17 July 2006; received in revised form 29 March 2007; accepted 9 April 2007

Available online 24 May 2007

Abstract

In this paper, a natural convection micro cooling system with a capillary microgroove evaporator is proposed. An experimental study on the characteristics of thermal resistance, pressure drop and heat transfer of the cooling system is carried out. Experimental results indicate that the liquid fill ratio has a significant influence on thermal resistance and heat transfer in the cooling system. Increasing system's cooling capacity at higher input power depends on decreasing the thermal resistance between the outer surfaces of the condenser and ambient environment. Compared with a flat miniature heat pipe (FMHP) and a current fan-cooled radiator for CPU chip of Pentium IV, the present micro cooling system has a stronger heat dissipation capacity. Its best cooling performance at a surface temperature of heat source below 373 K reaches 1.68×10^6 W m^{-2} and the maximum heat transportation capacity is 131.8 W. The novel kind of cooling system is suitable for remote cooling of those electronic parts with micro size, high power and thermal sensitivity.

Keywords: Cooling system; Microgroove; Evaporator; Thermal resistance; Pressure drop; Liquid fill ratio

1. Introduction

As new technology in the field of microchannel phase-change heat transfer, open capillary microgroove heat sink can drive fluid flow by capillary force and create enhanced phase-change heat transfer conditions by promoting the formation of an extended meniscus in each microgroove. The extended meniscus is typically divided into three regions: the intrinsic meniscus region; the evaporating thin film region; and the adsorbed layer. Intensive pure evaporation of thin liquid films occurs in the three-phase contact-line region (the junction of the evaporating thin film region and the adsorbed layer) at lower input heat load while combined heat transfer of evaporating heat transfer in the three-phase contact-line region and boiling heat transfer in the intrinsic meniscus region happens at higher input heat load. It has been used to achieve heat exchanges with high heat transfer coefficients and high heat fluxes [1–4].

Previously, heat pipe is an effective heat transfer device in which the thin liquid film evaporating heat transfer is realized by porous wick structure. For cooling micro electronic components, micro heat pipe concept was proposed by Cotter [5] in 1984. Afterward, it was verified experimentally by Babin et al. [6]. For cooling high heat flux electronic devices, Plesch et al. [7] then developed flat miniature heat pipes (FMHP). However, in a heat pipe the liquid and vapor are usually in direct contact and are flowing in opposite directions. The high-velocity vapor exerts a drag force on the liquid. If this drag force is sufficiently high, some of the returning liquid condensate can become entrained or trapped in the vapor passage and thus reduce the amount of liquid in the wick flowing to the evaporator section. This could lead to dryout of the wick in the evaporator section and overheating. In addition, the boiling limitation of heat pipe heat transport usually occurs for high-heat-flux applications in which boiling of the working fluid in the wick may form a vapor blanket on the evaporator inner surface and prevent it from being rewetted with returning liquid flow.

Like the heat pipes, Capillary Pumped Loops (CPLs) and Loop Heat Pipes (LHPs) are also passive, two-phase heat transport systems that utilize the capillary pressure developed in a fine pore evaporator wick to circulate the system's working fluid. The loops work well against gravity [8,9], use smooth

* Corresponding author. Tel.: +86 10 62573334; fax: +86 10 62575913.
E-mail address: xuegonghu@mail.etp.ac.cn (X. Hu).

1290-0729/$ – see front matter
doi:10.1016/j.ijthermalsci.2007.04.002

Nomenclature

$D_{v,\text{line}}$	vapor line diameter	m
d	groove depth	mm
F_{in}	front surface area of the heating cylinder	m^2
ΔH	altitude difference between the locations of the condenser and the evaporator	m
h_{fg}	latent heat of vaporization	J kg^{-1}
$L_{v,\text{line}}$	vapor line length	m
P_c	vapor pressure in the condenser	Pa
$P_{l,c}$	liquid pressure at the outlet of the condenser	Pa
$P_{v,e}$	vapor pressure at the outlet of the evaporator	Pa
Q_c	total condensation heat transfer quantity in the condenser	W
Q_e	total evaporation heat transfer quantity in the evaporator	W
Q_{in}	input power	W
Q_{out}	total heat dissipation quantity of the cooling system	W
q_{in}	input heat flux	W m^{-2}
R_1	thermal contact resistance between the front surface of the heater and the outer surface of the evaporator wall	K W^{-1}
R_5	vapor flow thermal resistance in the vapor line	K W^{-1}
R_9	thermal resistance between the outer surfaces of the condenser and ambient environment	K W^{-1}
R_c	total thermal resistance in the condenser	K W^{-1}
R_e	total thermal resistance in the evaporator	K W^{-1}
R_{sys}	total thermal resistance in the system	K W^{-1}
R_{total}	total thermal resistance of the system	K W^{-1}
s	groove pitch	mm
T_c	vapor temperature in the condenser	K
$T_{c,\text{wo}}$	temperature of the fin root on outer surface of the condenser	K
$T_{e,\text{wo}}$	temperature of the outer heated surface of evaporator wall	K
T_h	temperature of the front surface of the heater	K
$T_{l,e}$	temperature of liquid at the inlet of the evaporator	K
T_o	ambient temperature	K
$T_{v,e}$	temperature of vapor at the outlet of the evaporator	K
ΔT	temperature difference between two measuring points	K
w	groove width	mm
z	height of liquid level	cm

Greek symbols

δ	distance between two temperature measuring points	m
λ	thermal conductivity	$\text{W m}^{-1}\,\text{K}^{-1}$
ϕ	liquid fill ratio	
μ_v	vapor dynamic viscosity	Pa s
ρ_v	vapor density	kg m^{-3}

wall tubing for the transport lines making them easily routable [10,11], can handle high heat fluxes and can transport large heat loads over long distances [12,13]. They differ from conventional heat pipes in the following manner: (1) they are arranged in a loop. (2) The vapor and liquid flows are separated and are in the same direction. (3) High capillary pumping. (4) The wick structure is only required in the evaporator section. Consequently, smooth wall tubing can be employed in the construction of the vapor and liquid transport lines as well as in the condenser zone, which avoids the significant liquid flow losses in the wick materials experienced in a conventional heat pipe. However, Maidanik [14] and Kaya et al. [15] showed boiling limitation also easily occurs in the loops due to the complex wick structure. Moreover, the wick complexity also leads to large heat leaking and high pressure drop, which would severely restrict the heat transfer performance of the loops.

More recently, a novel cooling system for electronic devices by using a micro-open-capillary-groove evaporator was proposed by Hu et al. [16]. Different from CPLs and LHPs, this kind of system employs simple open capillary microgroove, instead of complicated wick structure, to create intensive phase-change heat transfer conditions in its evaporator. Working liquid is directly reservoired in the evaporator without an individual compensation chamber. These specialties result in no heat leaking and low pressure drop while keeping high passive capillary pressure as the pumping force. More importantly, it makes boiling in microgrooves helpful for improving thermal transport of the system. Hu et al. [16] reported that, the cooling performances reached a heat transfer capacity of 3.35×10^5 and $2.51 \times 10^5\ \text{W m}^{-2}$, respectively, for a desktop-type cooling system by using ethanol and a forced air-cooled condenser, and a notebook-type one by using methanol and a forced water-cooled condenser.

In the present paper, a new natural air-cooled micro cooling system with a vertical capillary microgroove evaporator is described especially for the desktop-type CPU chip. Here, a natural air-cooled condenser is used to dissipate the heat out of micro cooling system. The main purpose of this work is to clarify the characteristics of thermal resistance, pressure drop and heat transfer in the cooling system experimentally.

2. Cooling system design

A schematic diagram of the proposed natural convection micro cooling system with a capillary microgroove evaporator is shown in Fig. 1. The closed cooling system includes a capillary microgroove evaporator, a vapor line, a liquid line and natural air-cooled condenser. There is an evaporator wall with dense vertical rectangular microgrooves on its inner surface. With the help of capillary force, liquid from the pool in the evaporator can be wicked up along the microgrooves to a heating region of

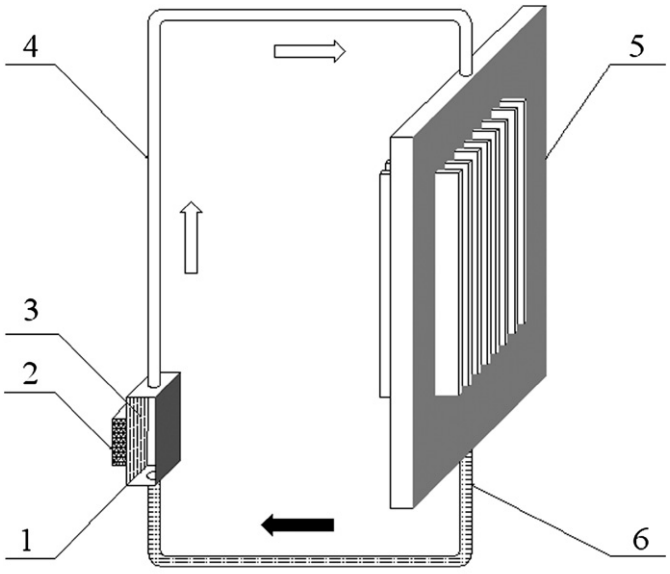

1. capillary microgroove evaporator
2. heating element
3. rectangular capillary microgrooves
4. vapor line
5. natural air-cooled condenser
6. liquid line

Fig. 1. Schematic of the micro cooling system.

the wall heated on the backside by a heating element for evaporation heat transfer. Along a vapor loop, evaporated liquid flows into a natural air-cooled condenser to be condensed, and then condensed liquid flows back along a liquid loop to the liquid pool of the evaporator under the action of gravity and capillary force. As a result of the cycle, high heat fluxes generated by heating electronic elements could be efficiently removed without any external power consumption.

The presented capillary microgroove evaporator is made of copper and its outline is cubiform. It is 56.0 mm high, 38.0 mm wide and 40.0 mm thick. There is an evaporation chamber in the evaporator. The wall thickness of the evaporator is 2.0 mm. The capillary microgrooves are manufactured by a wire-cut method. The length of each vertical microgroove is 52.0 mm. Its width is set at $w = 0.2$ mm, groove depth at $d = 0.7$ mm and groove pitch at $s = 0.2$ mm. The microgroove density is 2500 m^{-1}. The total microgroove number is 85 and the grooved section of the copper plate is 34.0 mm wide. To ensure the timely return of condensed liquid from the condenser, and to prevent the vapor outlet of the evaporator from being plugged by liquid drop, crisscross pattern rectangular microgrooves are arranged closely on the top and bottom surfaces of the evaporator. The configuration is displayed in Fig. 2. The microgrooves arranged in a crisscross pattern have the groove width of 0.2 mm, the groove depth of 0.7 mm and the groove pitch of 0.2 mm.

As shown in Fig. 3, the natural air-cooled copper condenser is thin wall-shaped. Its outline dimension is 250.0 mm high, 200.0 mm wide and 14.0 mm thick. A chamber exists in the condenser with a wall thickness of 3.0 mm. Small rectangular fins are fixed on the two outer side surfaces of the wall-

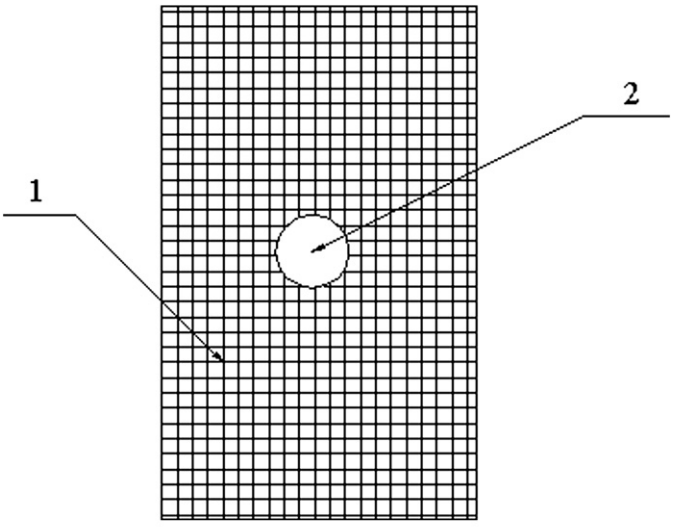

1. microgrooves arranged in a crisscross pattern
2. vapor outlet (liquid inlet)

Fig. 2. Configuration of the top (bottom) surface in the evaporator.

shaped condenser in order to enhance the natural convection heat transfer process happened between the cooling system and environment. Each fin is 200.0 mm long, 8.0 mm high and 1.0 mm thick. The fin pitch is 2.0 mm and the total width of the whole fin group is 172.0 mm. To enhance the condensation heat transfer process and to accelerate the drainage of condensed liquid, vertical microgrooves have been manufactured on the inner walls of the condenser. According to the numerical computation results [17], the optimal geometric shape of the microgroove should be with sharp edge, with gradually varying curvatures from the top to the root surface of the microgroove and with a wider width of groove for collecting condensed liquid. It is shown in Fig. 4. In the present work, the width between the tops of two neighboring microgrooves is 1.5 mm and the depth of each microgroove is 1.5 mm. Two slopes with many rectangular conducting grooves are located at the bottom in the condenser to accelerate the collection of condensed liquid with the help of gravity and capillary force. The width of the conducting groove is 1.5 mm, the depth 2.0 mm and the groove pitch 1.5 mm.

Smooth perfluoralkoxy tubes with an inside diameter of 3.0 mm are used as the vapor and liquid line in order to reduce pressure head loss for vapor or liquid flow and heat loss to environment.

3. Experimental setup

A schematic diagram of experimental setup is shown in Fig. 5. An electric heater was used to supply an input heat flux up to 500 W. The heater has a heating copper cylinder with the front surface diameter of 10.0 mm. The front surface is mounted on the outer surface of the evaporator wall. To reduce thermal contact resistance, Ag thermal silicone, whose thermal conductivity is above 2.9 $W\,m^{-1}\,K^{-1}$, was filled between their contact surfaces. In order to decrease heat loss to environment, the heat-

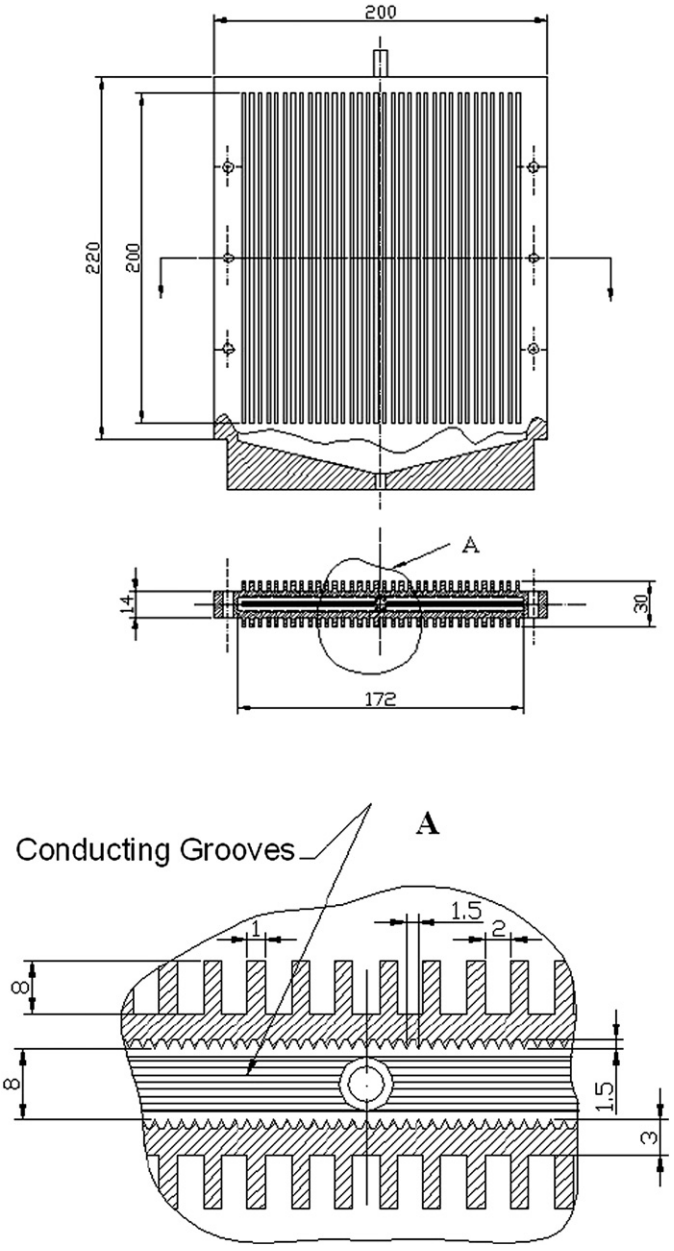

Fig. 3. Configuration of the natural air-cooled condenser.

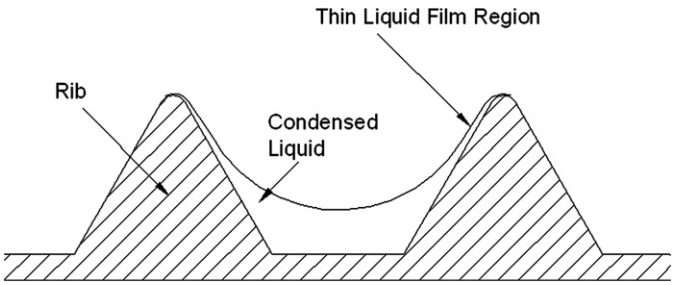

Fig. 4. Shape of mini-groove for condensation.

ing cylinder was packed in thermal insulating material. Along the axis of heating cylinder, three thermocouples were equidistantly placed. Input power Q_{in} or input heat flux q_{in} is given by

$$Q_{\text{in}} = F_{\text{in}} q_{\text{in}} = \lambda F_{\text{in}} \frac{\Delta T}{\delta} \tag{1}$$

Where F_{in} is the front surface area of the heating cylinder, ΔT is the temperature difference between two measuring points, λ is thermal conductivity of the heating copper cylinder and δ is the distance between the two points. The uncertainty of input power Q_{in} is less than ± 0.6 W and that of input heat flux q_{in} was estimated to be below $\pm 7.4 \times 10^3$ W m^{-2}. Other measured parameters in the present experiment include temperature of the outer heated surface of evaporator wall $T_{e,\text{wo}}$, temperature of liquid at the inlet of the evaporator $T_{l,e}$, temperature of vapor at the outlet of the evaporator $T_{v,e}$, temperature of the fin root on outer surface of the condenser $T_{c,\text{wo}}$, vapor pressure at the outlet of the evaporator $P_{v,e}$, vapor pressure in the condenser P_c and liquid pressure at the outlet of the condenser $P_{l,c}$. All thermocouples used in the present experiment are K-type with an experimental uncertainty of $\pm 0.1\,^{\circ}$C. The measuring range of the Pressure transducer is from 0 to 250 KPa. The uncertainty of Pressure transducer is $\pm 0.5\%$. A data logger (Agilent 34970A) was employed to record temperature and pressure data.

The thermal contact resistance between the front surface of the heater and the outer surface of the evaporator wall, R_1, is expressed as

$$R_1 = \frac{(T_h - T_{e,\text{wo}})}{Q_{\text{in}}} \tag{2}$$

where, T_h is the temperature of the front surface of the heater, $T_{e,\text{wo}}$ the temperature of the outer heated surface of evaporator wall and Q_{in} the input power. The total thermal resistance in the evaporator, R_e, is as follows

$$R_e = \frac{(T_{e,\text{wo}} - T_{v,e})}{Q_e} \tag{3}$$

where, Q_e is the total evaporation heat transfer quantity in the evaporator and $T_{v,e}$ is the temperature of vapor at the outlet of the evaporator. The total thermal resistance in the condenser, R_c can be obtained by

$$R_c = \frac{(T_c - T_{c,\text{wo}})}{Q_c} \tag{4}$$

where, T_c is vapor temperature in the condenser, $T_{c,\text{wo}}$ the temperature of the fin root on outer surface of the condenser and Q_c the total condensation heat transfer quantity in the condenser. The thermal resistance between the outer surfaces of the condenser and ambient environment, R_9, is calculated by

$$R_9 = \frac{(T_{c,\text{wo}} - T_o)}{Q_{\text{out}}} \tag{5}$$

where, T_o is ambient temperature and Q_{out} is the total heat dissipation quantity of the cooling system. The total thermal resistance of the system, R_{total}, is as follows

$$R_{\text{total}} = R_1 + R_e + R_5 + R_c + R_9 \tag{6}$$

It includes R_1 and R_9 while the total thermal resistance in the system, R_{sys}, is expressed by

$$R_{\text{sys}} = R_e + R_5 + R_c = \frac{T_{e,\text{wo}} - T_{c,\text{wo}}}{Q_{\text{in}}} \tag{7}$$

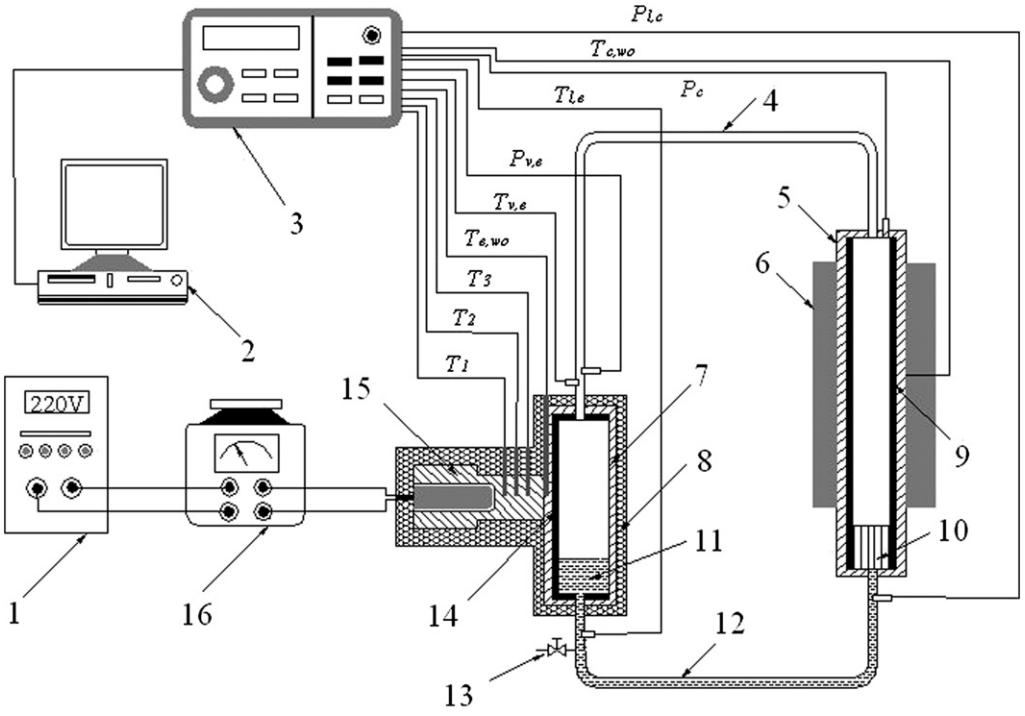

1. power supply 2. computer 3. data logger
4. vapor line 5. condenser 6. fin
7. evaporator 8. heat insulation layer 9. condensation grooves
10. conducting grooves 11. pool liquid 12. liquid line
13. vacuum valve 14. evaporation microgrooves 15. electric heater
16. transformer

Fig. 5. Schematic of experimental setup.

The difference between R_{sys} and R_{total} is

$$R_{\text{total}} = R_1 + R_{\text{sys}} + R_9 \tag{8}$$

Here, R_5 is the vapor flow thermal resistance in the vapor line,

$$R_5 = \frac{128\mu_v L_{v,\text{line}} T_c}{\pi D_{v,\text{line}}^4 \rho_v^2 h_{fg}^2} \tag{9}$$

where, μ_v is the vapor dynamic viscosity, $L_{v,\text{line}}$ the vapor line length, $D_{v,\text{line}}$ the vapor line diameter, ρ_v the vapor density and h_{fg} the latent heat of vaporization.

The total heat loss from insulation of the heating element, evaporator, and, moreover, the system overall is estimated to be lower than 4%. Therefore, the heat loss is negligible. Thus,

$$Q_{\text{in}} = Q_e = Q_c = Q_{\text{out}} \tag{10}$$

In the present experiments, ethanol, distilled water and methanol are used as working liquids. The cooling system is vacuumized. Liquid fill ratio ϕ is defined as the ratio of the volume of liquid filled in the system and the volume of the chamber in the evaporator. When experimental system reaches thermal steady state, experimental data is recorded for analyzing experimental results.

4. Results and discussion

4.1. Pressure drop

The pressure drop between the evaporator and the condenser leads to vapor flow from the evaporator to the condenser. Fig. 6 presents the variations of the pressure drop with input power. Under lower input power conditions, vapor mass flux increases as input power increases. It leads to a higher vapor pressure at the outlet of the evaporator while vapor can be condensed easily in the condenser. Thus, the pressure drop increases as input power increases. Under moderate input power conditions, however, the deteriorating condensation condition induces a high vapor pressure in the condenser. As a result of it, the pressure drop decreases as input power increases. Nevertheless, for higher input power cases, intensive phase-change heat transfer occurred in vertical microgrooves in the evaporator results in a sharp rise in vapor pressure at outlet of the evaporator. Therefore, the pressure drop continues to increase as input power increases. As shown in Fig. 6, for a too low liquid fill ratio case of 0.227, the distance between the pool liquid surface in the evap-

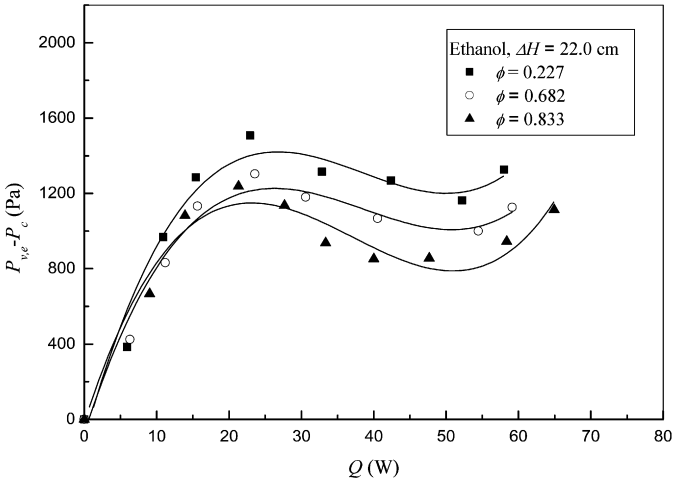

Fig. 6. Variations of pressure drop with input power.

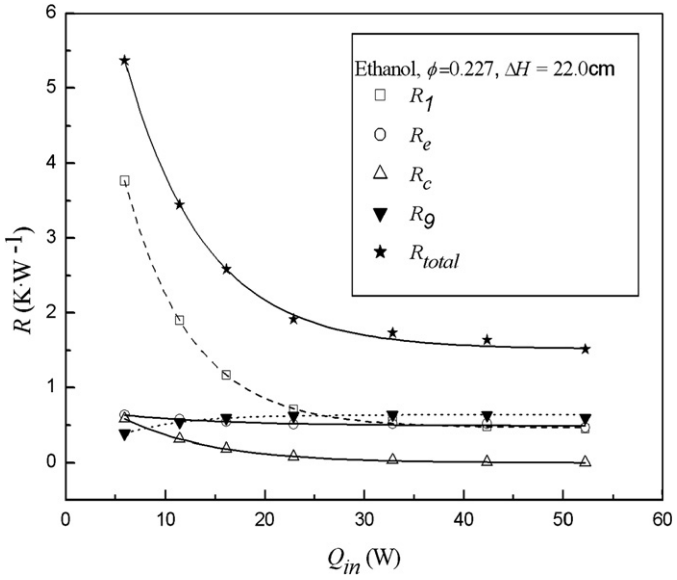

Fig. 7. Comparison of thermal resistances.

orator and the heating region of the wall heated on the backside by a heating element is too long. It increases the resistance to flow up to the heating region, thereby making evaporated fluid replacement difficult. As a result of it, average evaporation heat transfer coefficient decreases at high input power and the total thermal resistance in the evaporator becomes large. It leads to a higher vapor temperature and pressure in the evaporator than that of other two cases while there is little influence of liquid fill ratio on the total thermal resistance and vapor pressure in the condenser at high input power. Thus, the pressure drop is the highest among the three cases listed in the figure at some input power.

4.2. Thermal resistance and heat transfer

The comparison of thermal resistances of main heat transfer processes is shown in Fig. 7. It can be seen that thermal contact resistance R_1 between the front surface of the heater and the outer surface of the evaporator wall, is the primary thermal

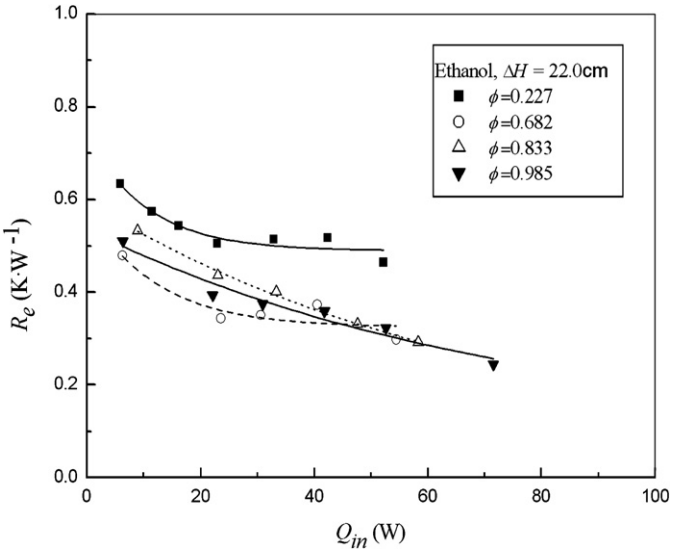

Fig. 8. Effect of liquid fill ratio on total thermal resistance in the evaporator.

resistance of the cooling system at lower input power cases. Under this condition, single-phase convection heat transfer and heat conduction through solid walls of the evaporator are dominating in the evaporator. The total thermal resistance of the system R_{total} is relative large. When input power continues to increase, however, the thermal contact resistance R_1 decreases sharply due to the influence of semifluid state of Ag thermal silicone which can improve the contact condition between the front surface of the heater and the outer surface of the evaporator wall. And, the total thermal resistance in the evaporator R_e become small due to the dominating evaporation and boiling heat transfer process in the evaporator at higher input power. On the other hand, the timely condensation of vapor with an increasing mass flux in the condenser is helpful to wet a large condensation area fully and then can drain the condensed liquid quickly by the gravity. Hence, the total thermal resistance in the condenser R_c decreases while input power increases. In a word, the total thermal resistance of the system decreases as the input power increases. Thus, the heat dissipation capacity of the system becomes strong. At higher input power, increasing system's cooling capacity depends on decreasing the thermal resistance R_9 between the outer surfaces of the condenser and ambient environment.

The effect of liquid fill ratio on total thermal resistance in the evaporator is shown in Fig. 8. Here, the altitude difference between the locations of the condenser and the evaporator ΔH is 22.0 cm. In Fig. 8, it is obvious that the total thermal resistance in the evaporator is the smallest for the liquid fill ratio of 0.682 when input power is about below 50 W. Under this condition, for a too low liquid fill ratio case, the distance between the pool liquid surface in the evaporator and the heating region of the wall heated on the backside by a heating element is too long. It increases the resistance to flow up to the heating region, thereby making evaporated fluid replacement difficult. For a too high liquid fill ratio case, the area of evaporating thin liquid film region in the microgrooves is reduced. As a result of it, average evaporation heat transfer coefficient decreases and the total

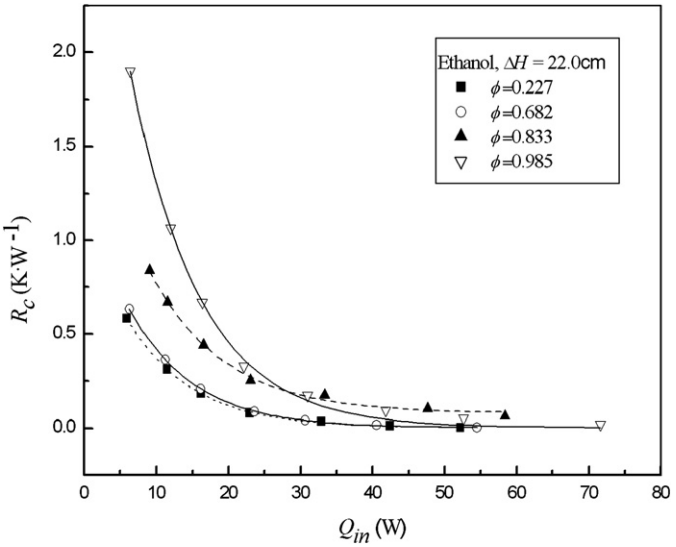

Fig. 9. Effect of liquid fill ratio on total thermal resistance in the condenser.

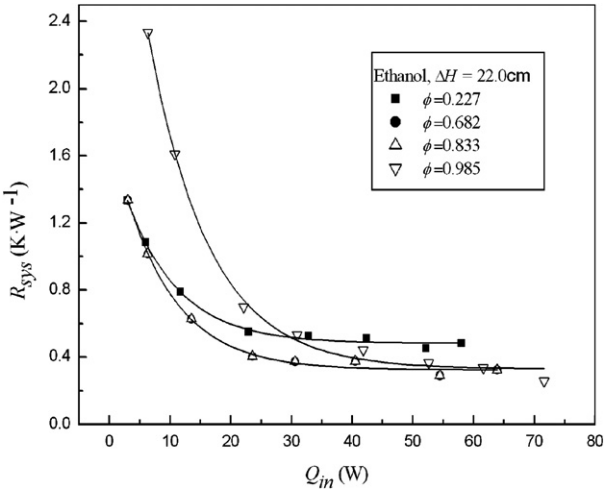

Fig. 10. Effect of liquid fill ratio on total thermal resistance in the cooling system.

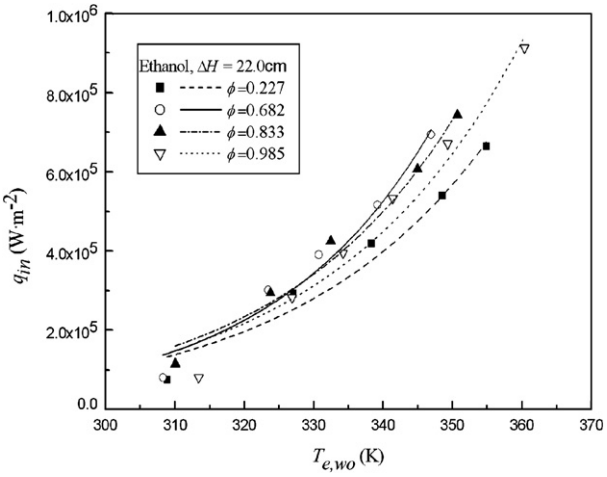

Fig. 11. Effect of liquid fill ratio on temperature of outer surface of the evaporator.

thermal resistance in the evaporator becomes large. Thus, an appropriate liquid fill ratio should be chosen for improving heat dissipation capacity of the system. While input power continues to increase, boiling heat transfer phenomena occurred in the intrinsic meniscus region in the microgrooves. Increasing liquid fill ratio is helpful for evaporating liquid to be supplied at very high vapor mass flux. And then, the total thermal resistance in the evaporator becomes small.

As shown in Fig. 9, the liquid fill ratio has an important effect on the total thermal resistance in the condenser. For a low liquid fill ratio case, a large evaporating thin liquid film area is easy to be created by the capillary force in the heating region of the microgrooves. It leads to an intensive evaporation heat transfer in the evaporator under a low input power condition and forms a high vapor mass flux to the condenser which is helpful to establish a good condensation condition in the condenser. Hence, the total thermal resistances in the condenser for the two relative low liquid fill ratios of 0.227 and 0.682 are smaller than those of other two relative high liquid fill ratios cases. It is shown in Fig. 9 that liquid fill ratio has little influence on the total thermal resistance in the condenser as input power becomes very high. Different from that at high input power cases, however, the condensation heat transfer condition is unsteady and susceptible to vapor mass flux when the input power is low. Varying liquid fill ratio can influence the distribution of thin liquid film in the heating region of microgrooves in the evaporator and thereby leading to the change of evaporated vapor mass flux to the condenser. Thus, the total thermal resistance in the condenser is severely dependent on the liquid fill ratio at low heat load cases.

In Fig. 10, it is apparent that the total thermal resistances in the system for the two liquid fill ratios of 0.682 and 0.833 (these symbols representing the two liquid fill ratio cases coincide each other in Fig. 10) are smaller than those for the two other liquid fill ratios as input power increases. Thus, it comes to the conclusion that it is important for enhancing the cooling performance of the present system to choose an appropriate liquid fill ratio.

The effect of liquid fill ratio on temperature of outer surface of the evaporator is displayed in Fig. 11. It is obvious that when input heat flux keeps constant, choosing an appropriate liquid fill ratio is helpful for decreasing the temperature of outer surface of the evaporator.

Fig. 12 shows the effect of various working liquids on total thermal resistance in the cooling system. Although the total thermal resistance in the cooling system using distilled water is higher when compared with those cooling systems using ethanol and methanol, it decreases sharply as input power increases. The thermal resistance for a case of ethanol is the lowest. The reason is that ethanol holds the best wetting characteristics among the three presented working liquids. Under the same heat input condition, Ethanol has a higher wetted height in the microgrooves of the evaporator and the condenser than the two other liquids. It makes the evaporated fluid replacement easy and the condensed liquid film thin. As a result of them, the average evaporation heat transfer coefficient and the average

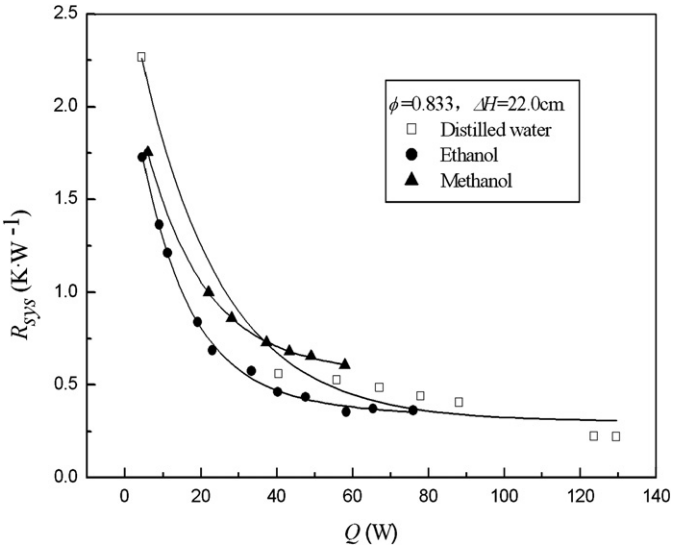

Fig. 12. Effect of various working liquids on total thermal resistance in the cooling system.

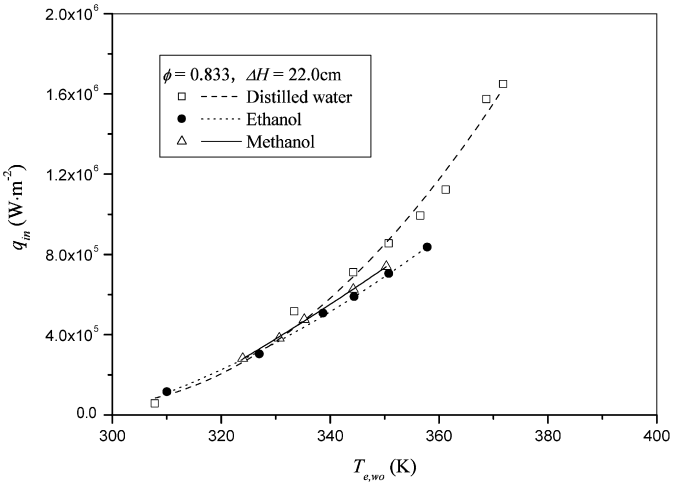

Fig. 13. Effect of various working liquids on temperature of outer surface of the evaporator.

condensation heat transfer coefficient increases, thereby lowing the total thermal resistance in the cooling system.

The effect of various working liquids on temperature of outer surface of the evaporator is showed in Fig. 13. Compared with those cooling systems using ethanol and methanol, the cooling system using distilled water has a stronger heat dissipation capacity at the same temperature of outer surface of the evaporator due to high latent heat value of distilled water.

4.3. Performance comparison with FMHP and fan radiator

Fig. 14 displays the experimental results of cooling performance comparison with a flat miniature heat pipe (FMHP) [18]. The FMHP is made of copper. Distilled water is used as working liquid for both systems. Liquid fill volume for the FMHP is 0.84 ml and liquid fill ratio for present cooling system is 0.833. The width of 0.2 mm of axial rectangular microgroove in the evaporator of the FMHP is the same as that of the present

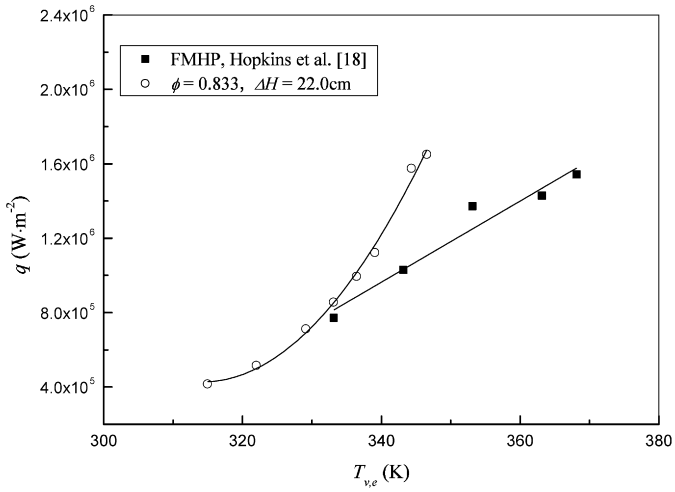

Fig. 14. Comparison of cooling performance with FMHP.

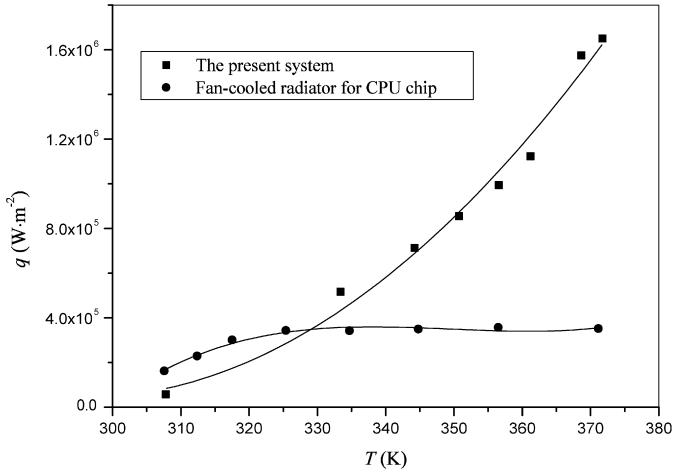

Fig. 15. Comparison of cooling performance with fan radiator.

cooling system. The depth of the microgroove is 0.42 mm, the groove pitch is 0.1 mm and total number of microgrooves is 62. The heated region of the FMHP is 0.7 cm^2 while the heated region of the present cooling system is 0.785 cm^2. The adiabatic region between the evaporator and the condenser of the FMHP is 70.0 mm. The length of its condenser is 34.4 mm. Different from the natural air-cooled method of the present cooling system, the FMHP uses forced water-cooled way to dissipate the heat out of the system.

In Fig. 14, it is obvious that input heat flux of the present cooling system can be far higher than that of the FMHP at the same operating temperature of system. It means that the present cooling system has a stronger cooling capacity due to no high frictional resistance to flow and pressure head loss.

Fig. 15 presents the experimental results of cooling performance comparison with a current fan-cooled radiator for CPU chip of Pentium IV. As shown in Fig. 15, the present natural convection micro cooling system by using a capillary microgroove evaporator has a stronger heat dissipation capacity. Its best cooling performance at the surface temperature of heat source below 373 K reaches a heat flux of 1.68×10^6 W m^{-2} and the maximum heat transportation capacity is 131.8 W while

a current fan-cooled radiator for CPU chip of Pentium IV removes the maximum heat load of 3.5×10^5 W m^{-2}.

In conclusion, the novel kind of cooling system is suitable for remote cooling of those electronic parts with micro size, high power and thermal sensitivity.

5. Conclusions

Input power and liquid fill ratio have complicated influences on the pressure drop between the evaporator and the condenser. In this work, the pressure drop is the highest for the case of a liquid fill ratio of 0.227 at the same input power.

Thermal contact resistance R_1 between the front surface of the heater and the outer surface of the evaporator wall is the primary thermal resistance of the cooling system at lower input power cases. And, the total thermal resistances in the evaporator and the condenser become very small at higher input power. At higher input power, increasing system's cooling capacity lies on decreasing the thermal resistance R_9 between the outer surfaces of the condenser and ambient environment.

Liquid fill ratio has a significant influence on thermal resistance and heat transfer in the cooling system. An appropriate liquid fill ratio should be chosen for improving heat dissipation capacity of the system.

The present natural convection micro cooling system by using a capillary microgroove evaporator has a strong heat dissipation capacity. Its best cooling performance at the surface temperature of heat source below 373 K reaches 1.68×10^6 W m^{-2} and the maximum heat transportation capacity is 131.8 W. The present cooling system is suitable for remote cooling of electronic parts with micro size, high power and thermal sensitivity.

Acknowledgements

The authors acknowledge the financial support provided by Funds of the Chinese Academy of Sciences for Key Topics in Innovation Engineering (Grant No. KGCX1-SW-12) and the National High Technology Research and Development Program of China (Grant No. 2006AA05Z225). The help of Prof. Yaohua Zhao is also gratefully acknowledged.

References

[1] A.K. Mallik, G.P. Peterson, Steady-state investigation of vapor deposited micro heat pipe arrays, ASME J. Electronic Packaging 117 (1995) 75–81.
[2] G.P. Peterson, A.B. Duncan, M.H. Weichold, Experimental investigation of micro heat pipes fabricated in silicon wafers, ASME J. Heat Transfer 115 (1993) 751–756.
[3] D. Khrustalev, A. Faghri, Enhanced flat miniature axially grooved heat pipe, ASME J. Heat Transfer 118 (1996) 261–264.
[4] R. Hopkins, A. Faghri, D. Khrustalev, Critical heat fluxes in flat miniature heat sinks with micro capillary grooves, ASME J. Heat Transfer 121 (1999) 217–220.
[5] T. Cotter, Principles and prospects of micro heat pipe, in: Proc. 5th International Heat Pipe Conference, Tsukuba, Japan, 1984, pp. 328–335.
[6] B.R. Babin, G.P. Peterson, D. Wu, Steady-state modeling and testing of a micro heat pipe, ASME J. Heat Transfer 112 (1990) 595–601.
[7] D. Plesch, W. Bier, D. Seidel, K. Schubert, Miniature heat pipes for heat removal from microelectronic circuits, in: D. Cho, R. Warrington Jr., et al. (Eds.), Micromechanical Sensors, Actuators, and Systems, in: ASME DCS, vol. 32, 1991, pp. 303–313.
[8] K. Goncharov, V. Kolesnikov, Development of propylene LHP for spacecraft thermal control, in: Proc. 12th International Heat Pipe Conference, Moscow–Kostroma–Moscow, Russia, 19–24 May 2002, pp. 171–176.
[9] T.D. Swanson, G.C. Birur, NASA thermal control technologies for robotic spacecraft, in: Proc. 12th International Heat Pipe Conference, Moscow–Kostroma–Moscow, Russia, 19–24 May 2002, pp. 26–34.
[10] J. Kirshberg, K. Yerkes, D. Liepmann, Micro-Cooler for chip-level temperature control, in: SAE Aerospace Power Systems Conference, Mesa, AZ, 1999, p. 341.
[11] A. Hoelke, H.T. Henderson, F.M. Gerner, M. Kazmierczak, Analysis of the heat transfer capacity of a micromachined loop heat pipe, in: Proc. the ASME Heat Transfer Division, HTD, vol. 364-3, 1999, pp. 53–60.
[12] J.T. Dickey, G.P. Peterson, Experimental and analytical investigation of a capillary pumped loop, J. Thermophys. Heat Transfer 8 (3) (1994) 602–607.
[13] M.T. North, D.B. Sarraf, J.H. Rosenfeld, et al., High heat flux loop heat pipe, Proc. Amer. Inst. Phys. Conf. 387 (1) (1997) 561–566.
[14] Y. Maidanik, N. Solodovnik, Y. Fershtater, Experimental and theoretical investigation of startup regimes of two-phase capillary pumped loop, Society of Automotive Engineers, Paper 93-2305, July, 1993.
[15] T. Kaya, J. Ku, Ground testing of loop heat pipes for spacecraft thermal control, in: 33rd AIAA Thermophysics Conference, Norfolk, VA, June 28 – July 1, 1999, AIAA-1999-3447.
[16] X.G. Hu, Y.H. Zhao, X.H. Yan, T. Tsuruta, A novel micro cooling system for electronic device by using micro capillary groove evaporator, J. Enhanced Heat Transfer 11 (4) (2004) 407–416.
[17] Y. Mori, K. Hijikata, S. Hirasawa, W. Nakayama, Optimized performance of condensator with outside condensing surface, ASME J. Heat Transfer 103 (1981) 96–102.
[18] R. Hopkins, A. Faghri, D. Khrustalev, Flat miniature heat pipes with micro capillary grooves, ASME J. Heat Transfer 121 (1999) 102–109.